

# Surface acoustic phonon modes of Ge nanocrystals embedded in SiO<sub>2</sub>

P.K. Giri<sup>a,\*</sup>, R. Kesavamoorthy<sup>b</sup>, B.K. Panigrahi<sup>b</sup>, K.G.M. Nair<sup>b</sup>

<sup>a</sup>*Department of Physics, Indian Institute of Technology Guwahati, Guwahati 781039, India*

<sup>b</sup>*Materials Science Division, Indira Gandhi Center for Atomic Research, Kalpakkam 603102, India*

Received 5 May 2005; received in revised form 10 June 2005; accepted 17 June 2005 by A.K. Sood

Available online 5 July 2005

## Abstract

Ge nanocrystals (NCs) embedded in SiO<sub>2</sub> are synthesized by ion implantation, and the surface vibrational modes of the Ge NCs are investigated using the low-frequency Raman scattering (LFRS) technique. LFRS studies show distinct low-frequency Raman modes in the range 6.5–21.2 cm<sup>-1</sup> for the Ge NCs depending on the implant dose and annealing temperature. These low-frequency Raman modes are attributed to the confined surface acoustic phonon modes of Ge NCs with (0,0) spheroidal mode and (0,3) torsional modes. Our results are in excellent agreement with the recent theoretical predictions of surface vibrational modes in Ge NCs.

© 2005 Elsevier Ltd. All rights reserved.

PACS: 61.46.+w; 63.22.+m; 78.30.Am; 81.07.Bc

Keywords: A. Germanium nanocrystals; C. Low-frequency Raman scattering; D. Acoustic phonons; D. Ion implantation

## 1. Introduction

Group IV semiconductor nanocrystals (NCs) such as Si- and Ge-NCs have attracted much interest because of their potential applications in Si-based optoelectronics, nanophotonics, and electronic/optical memory devices. In contrast to Si NCs, Ge NCs show stronger confinement effect [1] resulting in a direct gap semiconductor nature [2]. However, studies have shown that optical properties of the Ge NCs are dominated by defects [3] rather than the predicted bulk properties of the NCs. Ge NCs based memory devices have shown great potentials for future memory devices since they exhibit high-speed programming and low-voltage operation as compared to Si NCs based devices [4]. However, contribution of interface traps in the charge storage mechanism has not been understood properly [5]. There

has been substantial controversy about the origin of intense visible photoluminescence (PL) from Ge NCs [6,7], since both the quantum confinement model and the defect model have been put forward to explain the PL emission characteristics. Hence, properties specific to quantum size effect and surface/surrounding effect on Ge NCs need to be identified properly.

Vibrational frequencies of a NC will differ from those of the bulk crystal, since the surface atoms experience different forces than those in the interior of the NC. Low-frequency Raman scattering has proved to be a powerful tool to monitor surface vibrational modes of embedded NCs [8]. While the optical Raman spectra of Ge NCs of different sizes have been reported [9], distinctive features of Raman modes dominated by surface atoms and those dominated by interior atoms have not been identified yet. In the low-frequency range, Raman modes whose frequencies increase with decrease in NC size have been reported for various metal [10] and semiconductor [8,11] systems, and were attributed to the distortion modes of a continuum sphere

\* Corresponding author. Tel.: +91 3612582703; fax: +91 3612690762.

E-mail address: [pravat\\_g@yahoo.com](mailto:pravat_g@yahoo.com) (P.K. Giri).

[12]. However, no studies have been reported on Ge NCs embedded in SiO<sub>2</sub> matrix. In a recent theoretical study, Cheng et al. [13] predicted that low-frequency (<50 cm<sup>-1</sup>) surface vibrational Raman modes of Ge NCs involve relatively large motion of surface atoms. Experimental determination of the low-frequency modes is often difficult since the scattering cross-section is quite low for small sized NCs, whereas for the larger size NCs low-frequency modes fall in a region where the Rayleigh tail dominates the scattering intensity. In this work, we present a detailed investigation of the surface vibrational modes of Ge NCs embedded in SiO<sub>2</sub> matrix. Our results are compared with the theoretically predicted phonon modes.

## 2. Experimental details

To prepare the Ge nanocrystals, 300 keV Ge<sup>+</sup> ions were implanted at room temperature on thermally grown SiO<sub>2</sub> films of thickness ~300 nm on Si(100) substrate with fluences  $3 \times 10^{16}$  (Ge1),  $1 \times 10^{17}$  (Ge2) and  $2 \times 10^{17}$  (Ge3) ions/cm<sup>2</sup>. Implanted and unimplanted SiO<sub>2</sub> layers were first heat treated at 800 °C for 1 h and further treated at 950 °C for 2 h in argon gas ambient. Evolution of the Ge NCs has been studied after each step of annealing by using X-ray diffraction (XRD), optical Raman and low-frequency Raman scattering (LFRS) techniques. A powder X-ray diffractometer was used to record the XRD spectra in the grazing incidence mode. Raman spectra were recorded in the backscattering geometry using vertically polarized 488 nm Ar<sup>+</sup> laser beam, double grating monochromator and cooled photo multiplier tube detector. Low-frequency Raman spectra were recorded from 5 to 40 cm<sup>-1</sup> at steps of 0.5 cm<sup>-1</sup>. Optical Raman spectra were recorded in the range 150–660 cm<sup>-1</sup> using the same Raman spectrometer.

## 3. Results and discussion

Fig. 1(a) shows a set of XRD patterns on annealed Ge2 and Ge3 samples. Curve 1 is obtained for Ge2 sample annealed at 800 °C, curves 2 and 3 are obtained with different grazing angle of incidence for Ge2 sample annealed at 950 °C, and curve 4 is for Ge3 annealed at 950 °C. A strong Bragg peak at 26.44° and a weak peak at ~27.4° (shown with arrow) in curve 1 correspond to GeO<sub>2</sub> and Ge (111) NCs, respectively. Due to the very small size of the NCs grown after annealing at 800 °C, Ge related peak in XRD patterns is very weak. After 950 °C annealing, Ge(111) peak became distinct due to larger size of the NCs as shown in curves 2 and 4. Curve 3 shows Ge (311) peak obtained with different angle (3°) of grazing incidence on Ge2 sample annealed at 950 °C. These results show that embedded Ge NCs of (311) and (111) orientations are formed after post-implantation annealing.

The optical Raman spectra of Ge1 sample shown in

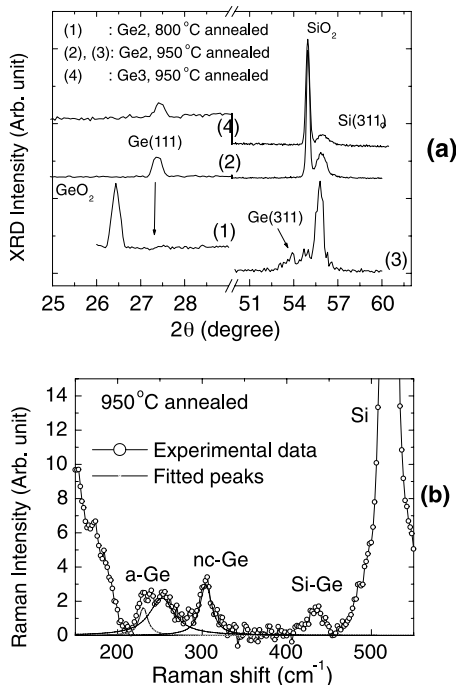


Fig. 1. (a) XRD patterns of Ge NCs formed by post-implant annealing at 800 °C for Ge2 (curve 1), and 950 °C (curve 2, 3 for Ge2, 4 for Ge3). Curve 2 and 3 are obtained for the same Ge2 sample under different grazing angle of incidence. (b) Optical Raman spectra of the 950 °C annealed samples implanted with Ge ions. Points in (b) are experimental data and solid line is the fit with Lorentzian line shapes. Bonds responsible for the modes are indicated.

Fig. 1(b) reveal peaks at 304 and 435 cm<sup>-1</sup> corresponding to scattering from optical phonons involving Ge–Ge and Si–Ge stretching motions, respectively [14]. The peak at 521.6 cm<sup>-1</sup> arises from the Si substrate, and weak peaks at ~230 and ~253 cm<sup>-1</sup> are signatures of Ge related components [15]. Using the phonon confinement model [15], the measured line width (15.1 cm<sup>-1</sup>) of the 304 cm<sup>-1</sup> Raman peak yields a size of 5.6 nm for the Ge NCs, which is similar to the size calculated from the LFRS spectrum (shown below).

Figs. 2 and 3 show LFRS spectra of Ge NCs prepared with different Ge<sup>+</sup> fluences ( $3 \times 10^{16}$ – $2 \times 10^{17}$  ions/cm<sup>-2</sup>) and subsequent heat treatment at 800 and 950 °C, respectively. They are fitted to Lorentzian line shapes and a background. Table 1 gives Lorentzian peak positions and the calculated (vide infra) Ge NC diameters. For a particular fluence, Ge NCs grow on increasing the annealing temperature. Ge NC size reaches maximum for a fluence of  $1 \times 10^{17}$  cm<sup>-2</sup>. As 800 °C annealed Ge1 sample contains too few small sized Ge NCs (Table 1), Raman intensity is expected to be low. SRIM calculation, a Monte Carlo code, of ion profile shows that 300 keV Ge<sup>+</sup> ions have a mean range of ~205 nm with a straggling of ~60 nm in SiO<sub>2</sub>.

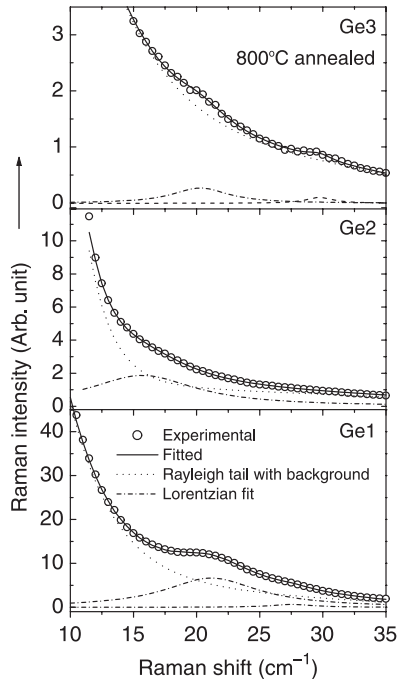


Fig. 2. Low-frequency Raman spectra of 800 °C annealed samples implanted with fluences  $3 \times 10^{16}$  (Ge1),  $1 \times 10^{17}$  (Ge2),  $2 \times 10^{17}$  (Ge3) ions/cm<sup>2</sup>. Points are experimental data, solid line is the fit with Lorentzian line shapes (broken lines) and background (dotted line).

Therefore, the Ge NCs are embedded inside the thermally grown SiO<sub>2</sub> layer.

X-ray diffraction analysis shows that Ge NCs are surrounded by SiO<sub>2</sub>/GeO<sub>2</sub> that impedes the vibration of the Ge atoms at the surface of the NC. In the calculation of the low-frequency Raman modes, NCs are assumed to have stress free surface or a sharp change in acoustic impedance  $z = \rho c$  at the NC–SiO<sub>2</sub> boundary. In contrast to the case of Si NCs embedded in SiO<sub>2</sub>, Ge NCs satisfy this condition since they are much heavier than the SiO<sub>2</sub> matrix. In predicting the surface vibrational modes of Ge NCs, Cheng et al. [13] assumed that surface atoms are those which have at least one dangling bond and a large motion of the surface atoms gives rise to Raman modes below 50 cm<sup>-1</sup>. Hence, the observed low-frequency Raman modes are attributed to the surface acoustic vibrational modes of Ge NCs [13].

Table 1

Low-frequency Raman peak positions  $\nu_s$  (for spheroidal (0,0) mode) and  $\nu_t$  (for torsional (0,3) modes) and their ratio ( $\nu_s/\nu_t$ ), and the calculated NC size,  $d$ , from the spectra shown in Figs. 2 and 3

Dose (cm <sup>-2</sup> )	800 °C annealing				950 °C annealing			
	$\nu_s$ (cm <sup>-1</sup> )	$\nu_t$ (cm <sup>-1</sup> )	$\nu_s/\nu_t$	$d$ (nm)	$\nu_s$ (cm <sup>-1</sup> )	$\nu_t$ (cm <sup>-1</sup> )	$\nu_s/\nu_t$	$d$ (nm)
$3 \times 10^{16}$	21.2	27.6	0.77	4.0	13.8	17.6	0.78	6.1
$1 \times 10^{17}$	15.7	–	–	5.4	6.5	9.8	0.66	13.0
$2 \times 10^{17}$	20.3	29.7	0.68	4.1	9.2	–	–	9.2

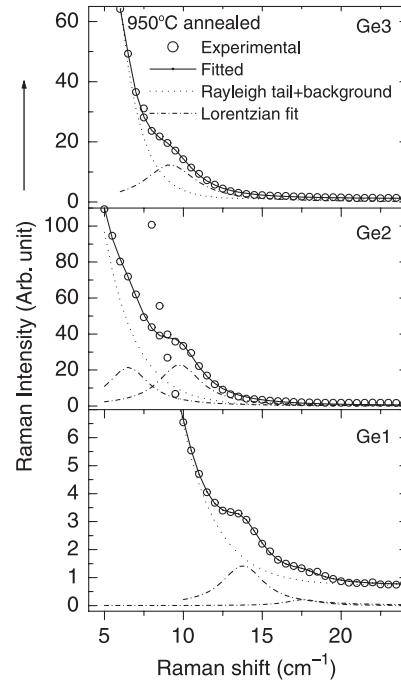


Fig. 3. Low-frequency Raman spectra of the Ge1, Ge2 and Ge3 samples after subsequent annealing at 950 °C. Points are experimental data, solid line is the fit with Lorentzian line shapes (broken lines) and background (dotted line).

We observed the LFRS peaks only in VV configuration when both incident and scattered rays are vertically polarized. These Raman results can be interpreted in terms of the vibrations of a homogeneous and spherical elastic body under different boundary conditions. These vibration modes can be classified as either spheroidal or torsional. The frequencies of these modes are quantized and depend on two integers: A branch number  $n$  and the angular momentum  $l$ , and a particular Lamb mode can be conveniently denoted as  $(n,l)$ . Only the lowest frequency modes with  $n=0$  in the spheroidal mode and  $n=0$  in the torsional mode correspond to the surface modes because these modes have large amplitudes near the surface of the NCs [13]. The higher frequency modes of  $n \geq 1$  correspond to the inner modes. The surface quadrupolar mode ( $l=2$ ) appears in both polarized and depolarized geometry, whereas the surface symmetrical mode ( $l=0$ ) appears only in the polarized

geometry. Our results are consistent with (0,0) spheroidal mode of acoustic phonons, since we observe LFRS peak only in the polarized geometry. Hence, we identify the lowest frequency mode in each sample as (0,0) spheroidal mode of surface acoustic phonons. For Ge NCs embedded in SiO<sub>2</sub> matrix, Cheng et al. [13] predicted that strongest contribution to spheroidal mode comes from (0,0) mode and to torsional mode from (0,3) mode. These two modes appear only in VV configuration [13]. Cheng et al. also showed that contributions from other low-frequency torsional modes ( $l$  values) would be very small [13]. Hence, we assign the high frequency mode to (0,3) torsional surface acoustic mode. The Raman shift  $\nu_1^S$  and  $\nu_1^T$  corresponding to spheroidal (0,0) and torsional (0,3) modes, respectively, are given by [11]

$$\nu_0^S = 0.78 \frac{v_t}{dc} \quad (n = 0) \quad (1)$$

$$\nu_3^T = 1.23 \frac{v_t}{dc} \quad (n = 0) \quad (2)$$

where  $c$  is the velocity of light,  $d$  is the average diameter of the NCs, and  $v_t$  is the transverse velocity of sound in Ge NCs. As per our assignment, theoretically predicted ratio  $\nu_0^S/\nu_3^T$  would be 0.634 if the modes arise from the same Ge NC. From our experimental data shown in Figs. 2 and 3, and the data presented in Table 1, the observed ratio closely matches with the predicted value for Ge2 and Ge3 samples. In case of Ge1 sample where the sizes of the NCs are very small, experimentally determined ratio is slightly larger than the predicted value, perhaps due to the non-spherical shape of the small NCs. Hence, the observed two peaks are due to spheroidal (0,0) and torsional (0,3) modes of the spherical Ge NCs. The deviation of the NC shape from the perfect spherical form may cause changes in symmetry and allows the torsional modes to appear [16]. The torsional modes becomes the mixed modes of transverse and longitudinal nature and, therefore, possible to observe them by LFRS. Ovsyuk et al. [17] observed similar modes for Ge NCs embedded in GeO<sub>2</sub> with a frequency ratio of  $\sim 0.72$ . Eqs. (1) and (2) are used to calculate the average size of the Ge NCs for different fluence and annealing conditions, and shown in Table 1. We have assumed a  $v_t = 3.25 \times 10^5$  cm/s for Ge [13]. Calculated NC sizes vary in the range 4.0–13.0 nm depending on the dose and annealing temperature. It is observed that Ge2 sample shows largest size NCs after 950 °C annealing. NC size increases with dose up to  $1 \times 10^{17}$  cm<sup>-2</sup> red shifting the LFRS peak positions. It is found that NC size is smaller in highest dose sample as compared to the size obtained in intermediate dose sample. Note that we observed a black coating on the sample surface after the high dose implantation performed at a high dose rate (beam current). Although exact reason for obtaining smaller size NCs in highest dose sample is not clear, it is likely that due to this black carbon coating on the SiO<sub>2</sub> layer the corresponding sample received less dose than the expected

dose of  $2 \times 10^{17}$  ions/cm<sup>2</sup>. Since the size of the NCs depends on the ion dose and the Ge3 sample may have received effectively lesser dose than the Ge2 sample, the NC size in Ge3 sample is lesser than the size found in the later case. Note that our observation from photoluminescence measurement [18] is also consistent with the observation from LFRS studies and hence the observed effect is not an artifact of measurement. We found that line width of the LFRS peaks decrease with the increase of annealing temperature. It is partly related to the change in size distribution of the NCs with annealing, and may be partly related to the recovery of lattice damage in the SiO<sub>2</sub> matrix.

We have recently shown that these embedded Ge NCs exhibit two broad photoluminescence (PL) peaks centered at  $\sim 2.1$  and  $\sim 2.3$  eV related to Ge NCs and defects at the Ge/SiO<sub>2</sub> interface, respectively [18]. Time resolved photoluminescence studies revealed nanosecond decay dynamics [18] in agreement with theory [19], but the dynamics was primarily controlled by the defects at the surface/interface of the NCs. Our results show that despite the presence of defects the low-frequency Raman modes are not strongly affected by such defects, since the observed modes obey the Lambs theory [12] of frequency versus NC size. In the region of small sizes where many analytical techniques have limitations, LFRS provides a non-destructive and convenient means to determine the size of the NCs by studying their low-frequency Raman modes. However, theory [13] predicts that for NC sizes smaller than 4 nm, Lambs theory may not yield the correct frequency.

#### 4. Conclusions

We provide experimental evidence of surface vibrational modes of Ge NCs embedded in SiO<sub>2</sub>. Confined surface acoustic phonon modes of Ge NCs with (0,0) spheroidal mode and (0,3) torsional modes are observed in the frequency range 6.5–21.2 cm<sup>-1</sup>, as predicted by recent theoretical calculation. Sizes of the NCs are found to vary with ion fluence and post-implantation annealing temperature. Surface vibration mode arise as the NCs are embedded in a matrix, which offers the restoring force that limits the free rotation of the NCs. Despite the presence of defects at the NC surface, acoustic phonon modes are least affected by these defects. Our results are in excellent agreement with the recent theoretical predictions.

#### Acknowledgements

We are thankful to S. Sarma, A. Srinivasan, P. Magudapathy, S. Dhara, B. Sundaravel, S. Amirtapandian, and David for various helps during the course of this work.

## References

- [1] C. Bostedt, T. van Burren, T.M. Willey, N. Franco, L.J. Terminello, C. Heske, T. Moller, *Appl. Phys. Lett.* 84 (2004) 4056.
- [2] J.R. Heath, J.J. Shiang, A.P. Alivisatos, *J. Chem. Phys.* 101 (1994) 1607.
- [3] K.S. Min, K.V. Shcheglov, C.M. Yang, H.A. Atwater, M.L. Brongersma, A. Polman, *Appl. Phys. Lett.* 68 (1996) 2511.
- [4] T. Usuki, T. Futatsugi, N. Yokoyama, *Microelectron. Eng.* 47 (1999) 281.
- [5] L.W. Teo, W.K. Choi, W.K. Chim, V. Ho, C.M. Moey, M.S. Tay, C.L. Heng, Y. Lei, D.A. Antoniadis, E.A. Fitzgerald, *Appl. Phys. Lett.* 81 (2002) 3639.
- [6] Y. Maeda, *Phys. Rev. B* 51 (1995) 1658.
- [7] J. Zhang, X. Bao, Y. Ye, X. Tan, *Appl. Phys. Lett.* 73 (1998) 1790.
- [8] E. Duval, A. Boukenter, B. Champagnon, *Phys. Rev. Lett.* 56 (1986) 2052.
- [9] K.L. Teo, S.H. Kwok, P.Y. Yu, S. Guha, *Phys. Rev. B* 62 (2000) 1584.
- [10] M. Fujii, T. Nagareda, S. Hayashi, K. Yamamoto, *Phys. Rev. B* 44 (1991) 6243.
- [11] A. Tanaka, S. Onari, T. Arai, *Phys. Rev. B* 47 (1993) 1237.
- [12] H. Lamb, *Proc. London Math. Soc.* 13 (1882) 189.
- [13] W. Cheng, S. Ren, P.Y. Yu, *Phys. Rev. B* 68 (2003) 193309.
- [14] M.I. Alonso, K. Winer, *Phys. Rev. B* 39 (1989) 10056.
- [15] X.L. Wu, T. Gao, X.M. Bao, F. Yan, S.S. Jiang, D. Feng, *J. Appl. Phys.* 82 (1997) 2704.
- [16] N.N. Ovsyuk, V.N. Novikov, *Phys. Rev. B* 53 (1996) 3113.
- [17] N.N. Ovsyuk, E.B. Gorokhov, V.V. Grischenko, A.P. Shebanin, *JETP Lett.* 47 (1988) 298.
- [18] P.K. Giri, R. Kesavamoorthy, B.K. Panigrahi, K.G.M. Nair, *Solid State Commun.* 133 (2004) 229.
- [19] H.-Ch. Weissker, J. Furthmuller, F. Bechstedt, *Phys. Rev. B* 69 (2004) 115310.